

Warm pool thermodynamics from the Arabian Sea Monsoon Experiment (ARMEX)

Debasis Sengupta, Sindu R. Parampil, G. S. Bhat

Centre for Atmospheric and Oceanic Sciences, Indian Institute of Science,
Bangalore, India

V. S. N. Murty, V. Ramesh Babu

National Institute of Oceanography, Goa, India

T. Sudhakar, K. Premkumar

National Institute of Ocean Technology, Chennai, India

Y. Pradhan

University of Plymouth, U.K.

Debasis Sengupta, Centre for Atmospheric and Oceanic Sciences, Indian Institute of Science,
Bangalore, 560012 India. (dsen@caos.iisc.ernet.in)

Abstract. Before the onset of the summer monsoon, sea surface temperature (SST) of the north Indian Ocean warms to 30-32°C. Climatological mean mixed layer depth in spring (March-May) is 10-20 m, and net surface heat flux (Q_{net}) is 80-100 W/m² into the ocean. It has been suggested that observed spring SST warming is small mainly due to (a) penetrative flux of solar radiation through the base of the mixed layer (Q_{pen}) and (b) advective cooling by upper ocean currents. We estimate the role of these two processes in SST evolution from a two-week ARMEX process experiment in April-May 2005 in the the southeastern Arabian Sea. The upper ocean is stratified by salinity and temperature, and mixed layer depth is shallow (6 to 12 m). Current speed at 2 m depth is high even under light winds. Currents within the mixed layer are quite distinct from those at 25 m. On subseasonal scales, SST warming is followed by rapid cooling, although the ocean gains heat at the surface - Q_{net} is about 105 W/m² in the warming phase, and 25 W/m² in the cooling phase; penetrative loss Q_{pen} is 80 W/m² and 70 W/m². In the warming phase, SST rises mainly due to heat absorbed within the mixed layer, i.e. Q_{net} minus Q_{pen} ; Q_{pen} reduces the rate of SST warming by a factor of three. In the second phase, SST cools rapidly because (a) Q_{pen} is larger than Q_{net} , and (b) advective cooling is ~ 85 W/m². A calculation using time-averaged heat fluxes and mixed layer depth suggests that diurnal variability of fluxes and upper ocean stratification tends to warm SST on subseasonal time scale. Buoy and satellite data suggest that a typical premonsoon intraseasonal SST cooling event occurs under clear skies when the ocean is gaining heat. In this respect, premonsoon SST cooling in the north Indian ocean is different from that due to MJO or monsoon ISO.

1. Introduction

Seasonal mean sea surface temperature (SST) in the Indo-Pacific warm pool rarely exceeds 30°C. Several mechanisms have been proposed to explain why the frequency distribution of tropical SST is asymmetric about the mean, with warm SST being less likely than cool SST. Basin-wide SST regulation on seasonal and longer time scales involves one or more of the following processes, in addition to the distribution of surface fluxes and upwelling in the upper ocean: (a) penetration of shortwave radiation beneath the ocean mixed layer (e.g. *Lewis et al.* [1990]; *Siegel et al.* [1995]; *Sengupta et al.* [2002]); (b) removal of heat by wind driven upper ocean currents (e.g. *Sun and Liu* [1996]; *Loschnigg and Webster* [2000]; *Clement et al.* [2005]), and (c) enhanced evaporation over warm SST and redistribution of boundary-layer moisture or of elevated latent heating by large scale atmospheric circulation (*Hartmann and Michelsen* [1993]; *Wallace* [1992]).

Atmospheric convection and clouds change incident radiation and SST via local and remote influences, which can be rather involved. In the Pacific Ocean, east-west gradient of seasonal SST (as well as SST itself) determines the distribution of convection and surface winds, and wind-driven currents influence the SST gradient. This is true of the equatorial Indian Ocean as well, at least during dipole (or Indian Ocean zonal mode) events (*Saji et al.* [1999]; *Webster et al.* [1999]; *Murtugudde et al.* [1999]). Removal of heat by divergent upper ocean circulation is thought to be important for long-term SST regulation of the tropical Pacific warm pool (e.g., *Seager and Murtugudde* [1997]; *McPhaden and Zhang* [2002]; *Clement et al.* [2005]).

In the Indian Ocean, long-term net surface heat flux is positive (i.e. into the ocean) north of about 15°S; although there is paucity of *insitu* observations, it is clear that southward heat transport by ocean circulation must play an important role in basin-

wide SST regulation (e.g., see *Webster et al.* [1998]; *Chirokova and Webster* [2006] and references there). The seasonal SST of the north Indian Ocean, i.e. the Bay of Bengal (BoB) and eastern Arabian Sea (AS), warms by 2-4⁰C in spring (February to early May), reaching 30-32 °C (*Sengupta et al.* [2002]) prior to summer monsoon onset. Away from the equatorial region, the sky is mostly clear and surface winds are light over the north Indian Ocean in this season, and climatological net surface heat flux Q_{net} is 80-100 W/m² (*Josey et al.* [1999]). Upper ocean stratification is stable, with a climatological mixed layer depth of 10-20 m (*de Boyer Montegut et al.* [2004]). *Rao and Sivakumar* [2000] and *Loschnigg and Webster* [2000] suggest that observed seasonal SST warming is smaller than might be expected, partly because of advective cooling by Ekman flow to the south. On the other hand, *Sengupta et al.* [2002] used limited buoy observations during 1998-2000 from the BoB and eastern AS to show that the thermodynamics of the premonsoon shallow mixed layer and sub-mixed layer are quite different: Although seasonal mean Q_{net} is about 100 W/m², shortwave flux penetrating below the mixed layer ($Q_{pen} \sim 45$ W/m²) limits SST warming. A residual cooling Q_{res} (~ 25 W/m²) inferred from the temperature data is attributed to intermittent advection or entrainment. SST warms in response to $Q_{net} - Q_{pen} - Q_{res}$ (20-30 W/m²), whereas sub-mixed layer warming is mainly due to Q_{pen} .

On intraseasonal time scales, SST in the Indo-Pacific warm pool responds mainly to changes in surface heat flux associated with Madden-Julian oscillations (MJO) or summer monsoon intraseasonal oscillations (ISO; *Lau and Waliser* [2005]). SST warms due to surface heat gain when the sky is clear and winds are light, and cools mainly due to surface heat loss under organised atmospheric convection, when it is cloudy and windy (e.g., *Anderson et al.* [1996]; *Lau and Sui* [1997]; *Shinoda and Hendon* [1998]; *Sengupta and Ravichandran* [2001]; *Duvel et al.* [2004]). As SST warms and the mixed layer shallows

under a clear sky, penetrative radiation warms the subsurface. In cloudy and rainy conditions, enhanced surface wind stress deepens the mixed layer, entraining subsurface water (*Zhang and McPhaden* [2000]). SST can become somewhat lower than subsurface temperature at this time because of stable salinity stratification. Therefore entrainment does not appear to add to SST cooling due to surface heat loss (*Shinoda and Hendon* [1998]). Although intraseasonal warming and cooling of SST has been described mainly as a local response to surface fluxes of momentum, heat and freshwater, observations (*Sengupta et al.* [2001]; *Saji et al* [2006]), theory (*Wang* [2005]) and models (*Slingo* [2005]), all suggest that variability of cloudiness and wind, and therefore surface flux itself, involves air-sea interaction (*Hendon* [2005]). On the other hand, buoy data from the premonsoon Bay of Bengal and Arabian Sea (at about 15°N) show sustained SST warming, with episodes of subseasonal SST cooling even under clear skies when the ocean gains heat (*Sengupta et al.* [2002]) - in this respect the mechanism of springtime SST cooling appears to differ from that forced by MJO or monsoon ISO.

1.1. ARMEX premonsoon warm pool study - background

As a part of the Indian Climate Research Programme (*DST* [1997]), the Arabian Sea Monsoon Experiment (ARMEX) was designed to study physical processes in the upper ocean and the atmosphere, related to onset and variability of the summer monsoon. It was conducted in several phases during the premonsoon and monsoon seasons of 2002, 2003 and 2005 in the eastern Arabian Sea and contiguous Indian land. A general discussion of ARMEX goals and implementation, as well as salient results of the 2002 and 2003 campaigns, may be found in *Sanjeeva Rao* [2005].

The ARMEX April-May 2005 campaign focused on upper ocean processes at single location off Minicoy in the southeastern Arabian Sea. The large scale oceanographic setting

of the southeastern Arabian Sea is discussed in several observational and model studies. Broadly speaking, upper ocean flow in the premonsoon season is clockwise around the Lakshadweep (or Laccadive) high (*Bruce et al* [1994]); the seasonal downwelling associated with the Lakshadweep high is thought to be forced mainly by remote winds (*Shankar et al* [2002]). Relatively low saline near-surface water is transported from the interior or south Bay of Bengal in autumn and winter; the source of this freshwater appears to be rainfall and river runoff to the Bay during the preceding summer monsoon (*Rao and Sivakumar* [2000]; *Gopalakrishna et al.* [2005]; *Sengupta et al.* [2006] and references there).

The spring warming of the southeastern AS (and the eastern Bay of Bengal) begins in February, somewhat earlier than other parts of the Indian Ocean warm pool; further, the warmest premonsoon SST is generally found in this region (e.g. *Shenoi et al* [1999]; *Rao and Sivakumar* [2000]). This is attributed to the presence of a shallow layer of relatively fresh water in winter and early spring. Data from a May 2000 cruise suggest that the spatial extent of the warmest water coincides with that of the strong density stratification at the base of the shallow fresh layer (*Sanil et al* [2004]). ARMEX 2003 observations show the presence of shallow mixed layers, barrier layers and temperature inversions (*Shenoi et al* [2004], *Shankar et al* [2004]). In addition to salinity effects, the north Indian Ocean warm pool also becomes increasingly stably stratified by temperature from March through May, as the near-surface layer warms more than the subsurface ocean (*Sengupta et al.* [2002]). Heat budgets based on climatological temperature and surface fluxes suggest that premonsoon warming of the upper ocean is mainly due to surface heat gain (*Shenoi et al* [2002]) and advection; entrainment cooling is relatively small in this season (*Rao and Sivakumar* [2000]).

Recent work with ocean general circulation models supports the broad conclusion that premonsoon SST warming in the southeastern AS is mainly governed by surface heat flux, lateral advection and solar penetration. Some recent studies with relatively high resolution models (see Discussion), partly motivated by the ARMEX 2003 results, pay close attention to the effects of near-surface salinity stratification. They all agree on the importance of penetrative radiation below the mixed layer. For example, *Kurian and Vinayachandran* [2006] and *de Boyer Montegut et al.* [2007] suggest that Q_{pen} can be 50-60 W/m² in the premonsoon southeastern AS. However, consensus has yet to evolve on the relative importance of barrier layers, temperature inversions and entrainment vis-a-vis fluxes in model SST evolution (e.g., *Durand et al.* [2004]; *Masson et al* [2005]; *Prasanna Kumar et al.* [2005]; *Kurian and Vinayachandran* [2007]; *de Boyer Montegut et al.* [2007]).

Here we use a short dataset based on ship, surface buoy, and mooring observations from the ARMEX 2005 premonsoon campaign, supplemented by subsurface radiation measurements from ARMEX 2003, to study thermodynamics of mixed-layer temperature (or SST) evolution at a location in the southeastern Arabian Sea, about 40 km northwest of the small island of Minicoy in the Lakshadweep group (Fig 1). We examine the role of surface heat flux, penetrative radiation, and lateral advection in subseasonal SST evolution, with the help of available observations and a simple heat balance. The data and methodology is outlined in the next section. In Section 3 we present the results of the heat balance calculations, and discuss possible sources of uncertainty in the estimates. The main results and their implications are discussed in Section 4.

2. The ARMEX premonsoon warm pool in 2005 - observations and approach

The ARMEX current meter mooring DS7A was deployed from 21 April-4 May 2005 at 8.3°N, 72.67°E (Fig 1), 1 km from DS7, which is a part of the regular surface buoy network

maintained by the National Institute of Ocean Technology, Chennai. Both DS7 and DS7A telemetered three-hourly near-surface oceanographic and meteorological parameters. In 2005, sustained SST warming ($\sim 1.5 - 2.5^\circ\text{C}$ per month) is punctuated by two major cooling events in February and April, each lasting two weeks (Fig 2a, hereafter C_1 and C_2 respectively); there is large diurnal warming, reaching 2.5°C on some days. Our focus is on processes responsible for the subseasonal warming and cooling of SST during 21 April - 4 May (Fig 2b). We shall see below that data limitations preclude study of heat balance on diurnal time scale; however, the observations and heat balance estimates suggest the possibility that diurnal variability rectifies to longer time scales.

While planning ARMEX 2005, we anticipated strong thermal and haline stratification, as well as the likelihood of relatively small-scale structure in temperature or salinity (~ 100 km scale eddies, fronts) in the near-surface ocean. ARMEX mooring DS7A was equipped with current meters at 2, 7, 15 and 25 and 40 m depth, but the instrument at 40 m returned no data. In addition, a current meter (FSI 2D) was installed on DS7 at 2 m depth on 6 May. Mooring DS7A recorded three-hourly currents, temperature (T) and salinity (S) at depths of 2 and 7 m (Make: FSI 2D), and hourly currents at 15 and 25 m (Aanderaa RCM9). In order to estimate lateral heat advection in the upper ocean using observed currents, we made repeat CTD (Idronaut and SeaCAT) observations on *ORV Sagar Kanya* cruise SK219, at a central station C near DS7A, and at stations E, W, N and S, following a butterfly track (Figure 2c). The distance between C and any of the vertices E, W, N or S, is about 12 km; the time interval between successive casts at station C is 6-8 hours, while it is 12-14 hours at E, W, S and N. Net surface shortwave radiation Q_{sw}^{net} and net longwave radiation Q_{lw}^{net} are based on 10-minute averages from shipborne sensors (Eppley); sensible heat flux Q_{sens} and latent heat flux Q_{lat} are estimated

from buoy air temperature, humidity and windspeed, with stability-dependent air-sea exchange coefficients (*Zeng et al.* [1998]). Subsurface solar radiation away from the ship's shadow was measured at over 100 stations using a profiling radiometer (SeaWiFS Profiler Multi-channel Radiometer; SATLANTIC) and a surface unit, on cruise SK193 in May-June 2003; profiling radiometer measurements are not available in 2005. Therefore we use estimates of penetrative radiation (300-800 nanometre; *Pradhan et al.* [2005]) based on a regression of measured subsurface flux against ship-based surface radiation (300-3000 nm), developed from the 2003 observations (see below). Details of buoy and ship instrumentation, including subsurface radiation measurements, may be found in *Parampil* [2005].

We define the warming phase of SST as the period 21-27 April (midnight to midnight), and the cooling phase 29 April - 2 May (see Fig 2b; hereafter phases I and II). Windspeed is generally less than 3 m/s in phase I, increasing to 4-6 m/s in phase II (Fig 3a). There is no classical mixed layer in phase I (Fig 3b) - the upper ocean is stratified by both temperature and salinity right from the surface (about 2 m in the CTD profiles). There is a distinct well-mixed layer in phase II (Fig 3c). $D(t)$, the time-varying mixed layer depth (MLD) computed from CTD data (Fig 3d), is the depth at which density ρ exceeds density at 2 m depth by 0.05 kg/m^3 . MLD from this density-based criterion applied to individual CTD profiles (*de Boyer Montegut et al.* [2004]) is close to the depth of the isothermal layer, where temperature is less than that at 2m depth by 0.25°C . The depth-average temperature of the density-based mixed layer and the isothermal layer are therefore quite similar (Fig 3e); the calculations below pertain to the mixed-layer depth and temperature. The upper ocean is warmest on 29 April; the upper 10-20 m is warmer than 30°C in phase I, and the upper 20-25 m in phase II (Fig 4a). Salinity is generally lower than 34.9 in the

upper 30 m (Fig 4b). In April-May 2005 we find no inversions except a weak ($< 0.1^\circ\text{C}$), short-lived one on 30 April (Fig 4a), and no well-defined barrier layer (see Fig 3b,c).

Our heat balance calculations are based on the following quantities: $Q_{net} = Q_{sw}^{net} + Q_{lw}^{net} + Q_{lat} + Q_{sens}$, where Q_{sw}^{net} is net shortwave flux entering the ocean; $Q(z) = Q_{sw}^{net} (1 - \alpha) \exp(-z/\zeta)$ is net shortwave flux (total downwelling minus upwelling irradiance) at depth z , where attenuation depth ζ depends on water clarity; the factor $\alpha=0.58$ accounts for the absorption of infrared and red radiation in the upper two metres or so in clear ocean water (*Paulson and Simpson [1977]*).

As mentioned, there are no direct observations of subsurface radiation in 2005. Profiling radiometer measurements in spring 2003 at the ARMEX location showed relatively clear water - attenuation depth ζ is 19 m, with an uncertainty of 2 m; ζ was obtained by fitting an exponentially decaying function of depth to the profile of net downwelling irradiance below 2 m depth, very close to the location of the ARMEX 2005 observations (8.3°N , 72.67°E ; *Parampil [2005]*). The value $\alpha=0.58$ is consistent with directly measured irradiance at the surface from the surface unit of the SATLANTIC radiometer, and the irradiance at 2 m from the profiler. Empirical estimates of penetrative radiation based on regression against shipborne Q_{sw}^{net} on the 2003 campaign (when we have direct observations of subsurface radiation) have rms uncertainty of 17 W/m^2 at 10 m depth (Fig 5), with contribution from measurement errors at different solar angles as well as differences in water clarity across stations. The climatological premonsoon attenuation depth based on satellite-based chlorophyll concentration, and the algorithm of *Morel [1988]*, is about 22 m in the ARMEX region. Weekly satellite chlorophyll data (Fig 6) suggest that the upper ocean has comparable clarity off Minicoy in the premonsoon 2003 and 2005 ARMEX campaigns. We therefore use the regression relation developed from the 2003 observations

to estimate $Q(z)$ on the 2005 campaign from the available shipboard Q_{sw}^{net} measurements. Total penetrative radiation across the base of the mixed layer $Q_{pen}=Q(z = D)$.

The mixed-layer heat balance is

$$\int_{z=0}^{z=D(t)} \frac{\partial T}{\partial t} dz = \frac{Q_{net} - Q_{pen}}{\rho C_p D(t)} - \int_{z=0}^{z=D(t)} \left(u \frac{\partial T}{\partial x} + v \frac{\partial T}{\partial y} + w \frac{\partial T}{\partial z} \right) dz + \text{Mixing}, \quad (1)$$

where C_p , u , v and w are specific heat of seawater, and zonal, meridional and vertical components of velocity; we have estimates of Q_{net} , Q_{pen} and lateral advection $Q_{adv} = -\rho C_p \left[\int_{z=0}^{z=D(t)} \left(u \frac{\partial T}{\partial x} + v \frac{\partial T}{\partial y} \right) dz \right]$, but not vertical advection or mixing/entrainment.

The current speed at 2 m depth is 20-60 cm/s, flowing approximately southward until mid-May, generally to the right of the wind (Fig 7 a,b). Currents at 7, 15 and 25 m are available only from DS7A, 21 April to 4 May. Current speed at 7 m is generally less than at 2 m until 27 April, but quite close to that at 2 m after 28 April. Current direction at 2 and 7 m are quite different throughout, for reasons that are not clear. There is semidiurnal variability, possibly of tidal origin, with amplitude of 5-15 cm/s, at 2, 7 and 15 m depth (Fig 7 c,d), and occasional evidence of six-hourly variability, such as on 24-25 April. Note that 2 m current can be swift (Fig 7c) even under very low wind (Fig 3a, 7a). MLD in the warming phase is in the range 2-8 m, and in the cooling phase it is 7-16m (Fig 3c) - thus it appears that currents within the mixed layer are distinct from deeper currents (Fig 7 c,d), except possibly for some coherent variation on tidal time scale after 28 April. Current directions at 15 and 25 m are similar in the warming phase (Fig 7a). The 25 m flow might be associated with eddies of ~ 200 km scale seen in satellite sea surface height (Fig 8, after *Murty et al* [2006]). For the purposes of this study we use the full available time resolution of CTD data to estimate $D(t)$ as well as east-west and north-south temperature gradients at C, together with the full (not de-tided) currents to compute lateral advection.

The observed currents have some features not previously reported from the Indian Ocean, such as the (a) difference in direction between 2 and 7 m, (b) high near-surface speed under low winds, and (c) difference between mixed layer and sub-mixed layer. Available ARMEX observations are not adequate to understand these features; a brief discussion of the possible dynamics of near-surface flow is in Appendix A. We examined data from a moored array centered at 15 °N, 61 °E in the central Arabian Sea during October 1994 to October 1995 (*Weller et al* [2002]); there are short periods (a few days) in spring 1995 with substantial difference in current direction between 5 m and 10m depth.

3. The basic thermodynamics of SST evolution

The sky is mainly clear during ARMEX 2005; mean shortwave radiative flux entering the ocean Q_{sw}^{net} is about 240 W/m² (Fig 9a; Table 1). Mean Q_{pen} below the shallow mixed layer is 80 W/m² in phase I and 70 W/m² in phase II (Fig 9a). For comparison, typical Q_{pen} in the equatorial west Pacific is 15-30 W/m² (*Siegel et al.* [1995]). Q_{lat} (Fig 9b) falls from -85 W/m² in phase I to -155 W/m² in phase II because windspeed increases (Fig 3a) and relative humidity decreases from 76% to 71% (not shown). Mean Q_{lw}^{net} is -45 W/m² in phase I and -55 W/m² in phase I (Fig 9b). In phase I, mean Q_{net} is 105 W/m² (Fig 9c); the effective heat flux $Q_{eff}=Q_{net}-Q_{pen}$, responsible for mixed layer warming, is therefore only 25 W/m². In phase II, Q_{net} is 25 W/m², but Q_{eff} is -45 W/m². Although the ocean gains heat at the surface, solar penetration would lead to upper ocean cooling. Advection Q_{adv} is about 5 W/m² in phase I, but -85 W/m² in phase II, when it is the dominant cause of SST cooling (Fig 9d). We note that the value of Q_{adv} in the cooling phase is sensitive to choice of averaging dates, e.g., the mean Q_{adv} in the period mid-day 29 April to mid-day 3 May is -55 W/m². Horizontal temperature gradients are small during the first few days, but increase after 26 April (Fig 10). A ~50 m deep structure appears to

pass through the observing array during 26-30 April, with E-W temperature difference reaching $\sim 1^\circ\text{C}$ (gradient 4°C per 100 km) at 10-20 m depth on 28 April (Figs 4, 10). Note that Q_{adv} increases in magnitude well before the windspeed increases (28 April; Fig 9a), or the 7 m currents change direction abruptly (29 April; Fig 7a).

The evolution of mixed-layer temperature predicted from observed Q_{net} , Q_{pen} and Q_{adv} is reasonably close to observed temperature on subseasonal time scales (Fig 11a). This suggests that vertical advection or entrainment are of secondary importance to the heat balance. Support for this inference comes from the upper ocean temperature and salinity fields (Fig 4) - (a) there is no sustained upwelling, and (b) the near-surface ocean continues to warm through the abrupt deepening of the the mixed layer on 28 April. The warming rate in phase I is $\sim 4.5^\circ\text{C}$ per month, comparable to the intraseasonal warming rates found in the west Pacific warm pool during TOGA COARE (e.g., *Anderson et al.* [1996]). Although Q_{net} is somewhat larger and D is shallower than in COARE, large Q_{pen} reduces warming during ARMEX. In phase II, the mixed layer cools rapidly though Q_{net} is positive into the ocean. The rapid cooling at about -5°C per month is due to advection, and because Q_{pen} exceeds Q_{net} .

The rapid subseasonal SST cooling under clear skies, in the absence of organised atmospheric convection, is quite unlike the typical SST cooling in the Pacific during the active phase of MJO or in the Bay of Bengal during the active phase of summer monsoon ISO, when the ocean loses heat (e.g., *Zhang and McPhaden* [2000]; *Sengupta and Ravichandran* [2001]). Recall that the buoy observations analysed in *Sengupta et al.* [2002] suggest that episodic SST cooling under clear skies is not uncommon in the premonsoon north Indian Ocean. We examined the intraseasonal cooling events in DS7 SST data, C_1 (1-20 Feb) and C_2 (20 Mar-8 Apr), each lasting about 20 days (Fig 2a, Fig 12b). Since radi-

ation measurements are not available, daily Q_{sw}^{net} and Q_{lw}^{net} were calculated from satellite outgoing longwave radiation (OLR), based on the empirical relations of *Shinoda et al.*, [1998], modified as in *Sengupta et al.* [2001]: $Q_{sw}^{net} = Q_{ERBE} + 0.93 \times OLR_a$ where Q_{ERBE} is climatological monthly net insolation from the Earth Radiation Budget Experiment [*Li and Leighton*, 1997] and OLR_a is daily OLR anomaly. Turbulent fluxes were estimated from 3-hourly buoy winds, SST, air temperature and pressure using the *Zeng et al.* [1998] algorithm. Q_{sw}^{net} during C_1 and C_2 is about 250 and 240 W/m², indicating absence of convection; wind speed is generally between 2 and 5 m/s (Fig 12a), and Q_{lat} is 80 and 130 W/m²; Q_{net} is generally positive, with average values of 105 and 50 W/m² during C_1 and C_2 , though it is negative for two days during C_2 (Fig 12c). In the absence of other data, we do not know how much of the SST cooling is due to solar penetration and lateral advection. It appears that subseasonal SST cooling of the premonsoon Indian Ocean warm pool in the presence of large positive Q_{net} is a common occurrence. It has been noted in TOGA COARE that if the mixed layer is shallow, west Pacific SST can cool due to Q_{pen} exceeding a small positive Q_{net} (*Anderson et al.* [1996]; *Godfrey et al.* [1998]).

There are several sources of uncertainty in the ARMEX heat balance. First, we note that the presence of the ship's hull in a shallow mixed layer with moderately fast currents leads to a serious underestimate of near-surface salinity and temperature stratification in the CTD observations (Fig 13). The shallow diurnal warming and the salinity gradient between 2 and 7 m depth seen in the DS7A observations are poorly captured by CTD data. The vertical density gradient as well its diurnal variability is underestimated by the CTD (Fig 13c). Therefore the mixed layer depth $D(t)$ used in our calculations is likely to be somewhat too deep, specially in daytime. Second, both buoy salinity (Fig

13b) and current speed (Fig 7c) have semidiurnal (and occasionally six-hourly) variability, likely of tidal origin. Neither the diurnal cycle nor tides are adequately resolved in the CTD casts because the repeat time is 6-14 hours, depending on location. Finally, lateral temperature gradients in the east-west or north-south direction appear to be nonuniform. For example, gradient computed from stations E and W is somewhat different from that computed from E and C, or C and W (see below). Therefore errors in mixed layer depth, as well as penetrative and advective heat fluxes can arise from (i) underestimate of vertical gradients in CTD data, (ii) infrequent CTD sampling, (iii) estimation of lateral gradients of T from non-simultaneous CTD casts at E and W (N and S), and (iv) unresolved gradients of T, i.e. spatial scale of $T(x,y)$ is small compared to spacing between CTD stations.

The mismatch between the diurnal phase of predicted and observed temperature is likely to be mainly due to inadequate time resolution, and underestimate of shallow diurnal warming in CTD data at the central location C. The mismatch on 23-24 April is possibly also related to a short-lived change of $D(t)$ (Fig 3c) of unknown origin, and on 27-28 April to the passage of the temperature front (Figs 4, 10). To estimate error in Q_{adv} due to small-scale gradients of T, we computed $\frac{\partial T}{\partial x}$ from CTD data at stations E and C, and W and C; and $\frac{\partial T}{\partial y}$ from N and C, and S and C. The contribution of lateral advection is somewhat sensitive to the pair of stations chosen to estimate gradient: For example, Q_{adv} estimated from N-C, E-C is -70 W/m^2 and that from C-S, C-W is -100 W/m^2 in phase II. This translates to significant changes in the evolution of advective cooling (Fig 14a) and the rate of cooling of mixed layer temperature (Fig 14b). Our qualitative conclusions are not altered - the largest uncertainty in MLT is 0.4°C at the end of 30 April (Fig 14b). The time interval between successive CTD casts at E and W (or N and S) is about 4 hours.

We artificially moved the $\frac{\partial T}{\partial x}$ and $\frac{\partial T}{\partial y}$ time series by 4 hours relative to the velocity record. This had insignificant impact on Q_{adv} . To estimate possible impact of tides and internal waves, we smoothed the velocity and temperature gradient with a 12-hour running mean. This changed Q_{adv} to 2 W/m² in the warming phase and -60 W/m² in the cooling phase, compared to 5 and -85 W/m² in our original calculation (see Table 1). The difference of 25 W/m² is likely to be an upper bound on the error in Q_{adv} due to tides and long period internal waves.

In order to examine the influence of the diurnal cycle, we used $D(t)$ and fluxes smoothed with a 24-hour running mean in the calculations (instead of $D(t)$ and fluxes at the highest available time resolution). The predicted mixed layer temperature then has a distinct cool bias after 25 April (Fig 11b). This is because a large fraction of shortwave radiation entering the ocean is absorbed in a very shallow layer - thus daytime warming acts on a shallower layer than nighttime cooling. The rectified effect of diurnal variability of fluxes and upper ocean temperature is thought to increase the amplitude of SST intraseasonal variability, and possibly to warm the mean SST on longer time scales, in the Pacific warm pool (*Shinoda and Hendon* [1998]; *Shinoda* [2005]; *Bernie et al.* [2005]). The ARMEX dataset suggests that diurnal effects enhance the amplitude of intraseasonal variability, but (a) the CTD dataset does not have adequate resolution to capture diurnal variability and (b) the experiment is too short, to make a conclusive statement. Note that our analysis probably underestimates the effect of rectification because CTD data does not capture the full magnitude of shallow daytime warming (Fig 13).

4. Discussion

The premonsoon ARMEX 2005 data show several new physical features in the upper layers of the southeastern Arabian Sea warm pool. The density mixed layer depth is

very shallow in the first part of the experiment, with salinity and temperature nearly linearly stratified from the surface to a depth of tens of metres. In the second part of the experiment, the stratification begins at about 10 m depth (Fig 3). The moored current meter observations show large differences in current direction between 2 m and 7 m depth, and between 7 m and 15 m (or 25 m), not consistent with Ekman flow. Current speed in the mixed layer is moderately high even at very low wind speed, and quite distinct from that at 25 m. Momentum input from wind appears to be mainly confined to the near-surface layer, which slips over the subsurface ocean (Fig 7; *Woods* [2002]). However, the absence of a clear diurnal cycle in 2 m current speed *Woods* [2002] suggests that local wind stress is not the only forcing, or even the most important one. We are unable to understand these characteristics of the currents from available observations. Dynamical considerations (see Appendix A) suggest that upper ocean currents are a complex response to winds and near-surface density gradients.

The main focus of this study is SST thermodynamics. The shallow mixed layer warms rapidly on subseasonal time scale in phase I, and cools rapidly in phase II. We have shown that the warming and cooling are mainly governed by surface fluxes, penetrative sunlight and lateral advection. Previous observational studies of intraseasonal warming and cooling of SST in the north Indian Ocean, based on limited data from surface buoys and satellites, focus on the summer monsoon season. SST variability is attributed mainly to changes in net surface heat flux associated with the active and weak phases of the summer monsoon (e.g., *Sengupta et al.* [2001]). The mechanisms of subseasonal SST warming and cooling in the southeastern Arabian Sea during the premonsoon season of 2005 (Fig 11) are different in some respects. Net surface heat flux Q_{net} is positive in both phases I and II, but SST cools in phase II. Penetrative radiation Q_{pen} reduces warming by a factor of three

in phase I (Table 1); Q_{pen} and advective cooling are together responsible for the rapid SST cooling in phase II. Moored observations suggest prominent shallow diurnal warming (Figs 2, 13), but there is inadequate data to construct a diurnal heat balance. Although it is underestimated in CTD observations (Fig 13), our calculations suggest that variability of near-surface stratification and surface flux (Fig 9) on diurnal scale together rectify to warm SST on longer time scales (Fig 11). We find that intraseasonal SST cooling in the presence of positive Q_{net} appears to be common in the premonsoon Indian Ocean warm pool (see also *Sengupta et al.* [2002]).

Some of these results have significant implications for models of warm pool SST and climate. Present day ocean general circulation models give realistic SST on subseasonal and longer time scales if air temperature is specified from observations (e.g., *Kurian and Vinayachandran* [2007]; *de Boyer Montegut et al.* [2007]; Jerome Vialard, personal communication, 2006). However, most models are forced with daily-mean (or smoother) surface fluxes, and their vertical resolution is typically five or ten metres in the upper ocean. The ARMEX 2005 observations suggest that model resolution (and related mixing parameterisation), as well as time and space resolution of model surface forcing fields, might be inadequate to capture important physical processes in the Indian Ocean warm pool. This is particularly true in the presence of salinity stratification. The low saline water in the premonsoon southeastern Arabian Sea seen in the ARMEX observations is not due to local rainfall, but owes its origin to freshwater from Bay of Bengal rivers and monsoon rain (see *Gopalakrishna et al.* [2005]; *Sengupta et al.* [2006]). More observations and improved models are needed to determine if inhibition of vertical mixing allows Bay of Bengal surface freshwater to reach remote regions of the tropical Indian Ocean, where it might control warm pool SST.

Appendix A:

Under light winds and clear skies, the near-surface layer (upper few metres) of the tropical ocean warms in the daytime. A temperature gradient in the diurnal thermocline of $\sim 0.05^{\circ}\text{C}$ - 0.5°C per metre can have significant influence on the dynamics of the upper ocean. Diurnal warming can make the density stratification large enough to suppress turbulence (see chapter 4 of *Fedorov and Ginsburg* [1992]). Under these conditions, the "slippery" near-surface layer glides without friction over the deeper water (*Houghton and Woods* [1969]; *Woods* [2002]). Near-surface current can be swift even under light winds, because the turbulent stress (or momentum penetration from wind) is confined to a shallow layer. Intense daytime surface currents (a few tens of centimetres per second at ~ 0.5 m depth) have been reported from the tropical Pacific and Atlantic (*Fedorov and Ginsburg* [1992]; *Kudryavtsev and Soloviev* [1990]). The ARMEX 2005 observations do not have the fine space or time resolution necessary to distinguish laminar from turbulent flow in the stratified upper ocean; the required vertical resolution of T, S and current data to compute gradient Richardson number is tens of centimetres (John Woods, personal communication, 2007; section 10.3, *Turner* [1973]).

The near-surface ocean is strongly stratified by both S and T, at least in the warming phase. On subseasonal scale, 2 m and 7 m currents are generally different in phase I, but are highly coherent in phase II (Fig 7); the 2 m current is decoupled from the 15 m and 25 m currents throughout, except briefly on 23 April when the mixed layer is deep (Fig 3). The upper "mixed" layer appears to glide over the deeper layer in phase I, and perhaps throughout our experiment. This is consistent with momentum balance estimates on subseasonal time scale (see below). If upper ocean flow is effectively frictionless, it can accelerate to high speeds even under low winds. Reponse to local wind cannot be the full

story, however - DS7A moored data shows strong diurnal variation of T, S and density stratification, but 2 m current speed does not have clear diurnal modulation.

We examine upper ocean momentum balance. The stress distribution in the ocean is unknown; we assume that it is zero below 6 m (the mean MLD) in phase I. Then the local acceleration, coriolis ($-fv$, fu) and stress terms can be estimated from buoy winds and 2 m currents. We focus on time scales of a day and longer because tidal forcing is not known (a 12-hour running mean is used):

$$\frac{\partial u}{\partial t} - fv = \frac{\tau_x}{\rho D} + residual; \quad \frac{\partial v}{\partial t} + fu = \frac{\tau_y}{\rho D} + residual, \quad (\text{A1})$$

where τ_x , τ_y are zonal and meridional surface wind stress; the residual includes pressure gradient and penetration of eddy momentum flux (vertical divergence of stress) below the 6 m level. Local acceleration is small compared to coriolis acceleration; there is possibly some variability at inertial period, ~ 3.5 days at this latitude (Fig A1a,b). Zonal pressure gradient appears to be required to balance the coriolis term (Fig A1a). Meridional momentum balance (Fig A1b) suggests that eddy momentum flux penetrates below 6 m in phase II, after 27 April when τ_y increases abruptly: This would be consistent with change in (a) near-surface stratification and $D(t)$, and (b) coherence between 2 m and 7 m current speeds. There is thus a hint in the observations that the physics of the slippery layer is relevant on subseasonal scale.

It is harder to do a similar analysis for 7 m currents because we do not know subsurface stress. We assume that the residual from the 2 m meridional balance (Fig A1b) represents penetration of momentum below 6 m, and that the momentum penetrates to 14 m depth. The 7 m current shows southward acceleration after 27 April (Fig A1c), consistent with such a stress forcing. Momentum balance in this subsurface layer appears

to require a meridional pressure gradient. There are substantial near-surface zonal and meridional gradients of T and S in CTD data, with significant depth dependence (not shown). Near-surface pressure gradient might arise from density (S and T) gradients relative to subsurface depths (see *Gordon et al.* [2003]) but this cannot be deduced from CTD data (*Fedorov and Ginsburg* [1992]); in the absence of other evidence, it is a tentative conclusion. The ARMEX near-surface current is likely to be a response to the history of the wind forcing (via inertial effects), and to pressure gradient and stratification over the study region. It cannot be understood purely on the basis of local winds. More work is required to understand the dynamics of shallow currents in the warm pool.

Acknowledgments. We thank P. A. Geda of SAC Ahmedabad, ORV Sagar Kanya personnel, and all those who helped with organisation, mooring deployment and observations during the ARMEX cruises. This work is supported by the Departments of Science and Technology and Ocean Development, New Delhi. SRP thanks the Council for Scientific and Industrial Research, New Delhi. This is NIO contribution no. XXXX

References

- Anderson, S.P., R. A. Weller and R. B. Lukas, Surface buoyancy forcing and mixed layer of the western Pacific warm pool: Observations and 1D results, *J. Climate*, 9, 3056–3085, 1996.
- Bernie, D.J., S. J. Woolnough, J. M. Slingo and E. Guilyardi, Modeling diurnal and intraseasonal variability of the ocean mixed layer, *J. Climate*, 18, (8), 1190-1202, 2005.
- Bruce, J. G., D. R. Johnson, and J. C. Kindle, Evidence for eddy formation in the eastern Arabian sea during the northeast monsoon, *J. Geophys. Res.*, 99, 7651–7664, 1994.

- Chirokova, G., and P. J. Webster, Interannual Variability of Indian Ocean Heat Transport, *J. Climate*, 19, 1013–1031, 2006.
- Clement, A. C., R. Seager, and R. Murtugudde, Why are there tropical warm pools?, *J. Climate*, 18, 5294–5311, 2005.
- Duvel, J. P., R. Roca, and J. Vialard, Ocean Mixed Layer Temperature Variations Induced by Intraseasonal Convective Perturbations over the Indian Ocean, *J. Atmos. Sci.*, 61, 1004–1023, 2004.
- Durand, F., S. R. Shetye, J. Vialard, D. Shankar, S. S. C. Shenoi, C. Ethe and G. Madec, Impact of temperature inversions on SST evolution in the southeastern Arabian Sea during pre-summer monsoon season, *Geophys. Res. Lett.*, 31, doi:10.1029/2003GL018906.
- DST Indian Climate Research Programme, Science Plan, Department of Science and Technology (unpublished manuscript), 1997.
- de Boyer Montegut, C., G. Madec, A. S. Fischer, A. Lazar, and D. Iudicone, Mixed layer depth over the global ocean: An examination of profile data and a profile-based climatology, *J. Geophys. Res.*, 109, C12003, doi:10.1029/2004JC002378, 2004.
- de Boyer Montegut, C., et al., Simulated seasonal and interannual variability of mixed layer heat budget in the northern Indian Ocean, *J. Clim.*, *In press*, 2007.
- Fedorov, K. N. and A. I. Gisburg, The near-surface layer of the ocean, Utrecht: VSP.-III, 1992.
- Godfrey, J. S., et al., Coupled Ocean-Atmosphere Response Experiment (COARE): An interim report, *J. Geophys. Res.*, 103(C7), 14,395–14,450, 1998.
- Gopalakrishna, V.V., Z. Johnson, G. Salgonkar, K. Nisha, C.K. Rajan, and R.R.Rao, Observed variability of sea surface salinity and near-surface thermal inversions in the southeastern Arabian Sea during the winter following active and weak monsoon, *Geo-*

- phys. Res. Lett.*, 32, L18605, doi:10.1029/2005GL023280, 2005.
- Gordon, A. L., R. D. Susanto, K. Vranes, Cool Indonesian throughflow as a consequence of restricted surface layer flow, *Nature*, 425 (6960), 824–828, 2003.
- Hartmann, D. L., and M. L. Michelsen, Large-scale effects on the regulation of tropical sea surface temperature, *J. Climate*, 6, 2049–2062, 1993.
- Hendon, H., Air-sea interaction, in *Intraseasonal Variability in the Atmosphere - Ocean Climate System*, W. K. M. Lau and D. Waliser (Eds.), pp 223-242, Springer, 2005.
- Josey, J. A., E. C. Kent and P. K. Taylor, New Insights into the Ocean Heat Budget Closure Problem from Analysis of the SOC Air Sea Flux Climatology, *J. Climate*, 105, 3295–3306, 1999.
- Joseph, P. V., Warm pool over the Indian Ocean and monsoon onset, *Trop. Ocean-Atmos. Newslett.*, Winter, 1–5, 1990.
- Kudryavtsev, V. N., and A. V. Soloviev, Slippery near-surface layer of the ocean arising due to daytime solar heating, *J. Phys. Oceanogr.*, 20, 617–628, 1990.
- Kurian, J., and P. N. Vinayachandran, Formation mechanisms of temperature inversions in the southeastern Arabian Sea, *Geophys. Res. Lett.*, 33, L17611, doi:10.1029/2006GL027280, 2006.
- Kurian, J., and P. N. Vinayachandran, Mechanisms of formation of the Arabian Sea mini warm pool in a high resolution OGCM, *J. Geophys. Res.*, 112, C05009, doi:10.1029/2006JC003631, 2007.
- Li, Z. Q., and H. Leighton, Global climatology of the solar radiation budgets at the surface and in the atmosphere from 5 years of ERBE data, *J. Geophys. Res.*, 98, 4919–4930, 1993.

- Lau, K. M., and C. H. Sui, Mechanisms of Short-Term Sea Surface Temperature Regulation: Observations during TOGA COARE, *J. Climate*, 10, 465–472, 1997.
- Lau, W. K. M. and Waliser, D (Eds.), Intraseasonal Variability in the Atmosphere - Ocean Climate System, pp. 436, Springer, 2005.
- Lewis M., M. Carr, G. Feldmann, W. Essaias, and C. McClain, Influence of penetrating solar radiation on the heat budget of the equatorial Pacific Ocean, *Nature*, 347, 543–545, 1990.
- Loschnigg, J. and P. J. Webster, A coupled ocean-atmosphere system of SST modulation for the Indian Ocean, *J. Climate*, 13, 3342–3360, 2000.
- Masson et al., Impact of barrier layer on winter spring variability of the southeastern Arabian Sea, *Geophys. Res. Lett.*, 32, doi:10.1029/2004GL021980.
- McPhaden and Zhang, Slowdown of the meridional overturning circulation in the upper Pacific Ocean, *Nature*, 415, 7, 603–608, 2002.
- Morel, A., Optical modeling of the upper ocean in relation to its biogenous matter content (case I waters), *Geophys. Res. Lett.*, 93, 1652–1665, 1988.
- Murtugudde, R., J. P. McCreary Jr., and A. J. Basalacchi, Oceanic processes associated with anomalous events in the Indian Ocean with relevance to 1997-1998, *J. Geophys. Res.*, 105, 3295–3306, 1999.
- Murty, V. S. N., et al., On the warm pool dynamics in the southeastern Arabian Sea during April-May 2005 based on satellite remote sensing and ARGO float data, in *Remote Sensing of the Marine Environment, Proc. SPIE*, 2006. Available at <http://drs.nio.org/drs/handle/2264/548>
- Paulson, C. A. and J. J. Simpson, Irradiance measurements in the upper ocean, *J. Phys. Oceanogr.*, 7, 952–956, 1977.

- Parampil, S. R., Mixed Layer Thermodynamics of the southeastern Arabian sea using ARMEX observations, *M.Sc(Engg) Thesis*, 2005. Available at <http://caos.iisc.ernet.in/faculty/dsen.html>
- Pradhan, Y., M. Mohan, D. Sengupta, and S. Nayak, Radiant heating rates and surface biology during the Arabian Sea Monsoon Experiment, *J. Geophys. Eng.*, 2, 16–22, 10.1088/1742-2132/2/1/003, 2005.
- Prasanna Kumar, S., A. Ishida, K. Yoneyama, M. R. Ramesh Kumar, Y. Kashino and H. Mitsudera, Dynamics and thermodynamics of the Indian Ocean warm pool in a high-resolution global general circulation model, *Deep Sea Res. II*, 52, 2031–2047, 2005.
- Rao, R. R. and R. Sivakumar, Seasonal variability of near surface thermal structure and heat budget of the mixed layer of the tropical Indian Ocean from a new global ocean temperature climatology, *J. Geophys. Res.*, 105, 995–1015, 2000.
- Sanilkumar, K. V, P. V. Hareesh Kumar, J. Joseph and J. K. Panigrahi, 2004: Arabian sea mini warm pool during May 2000 *Curr. Sci*, 86, No.1, 180–184, 2004.
- Sanjeeva Rao, P., Arabian Sea monsoon experiment: An overview, *Mausam*, 56(1), 1-6, 2005.
- Saji, N. H., S. P. Xie and C. Y. Tam, Satellite observations of intense intraseasonal cooling events in the tropical south Indian Ocean, *Geophys. Res. Lett.*, 33, 14, 2006.
- Saji, N. H., B. N. Goswami, P. N. Vinayachandran and T. Yamagata, A dipole mode in the tropical Indian Ocean, *Nature*, 401, 6751, 360–363, 1999.
- Seager, R., and R. Murtugudde, 1997: Ocean Dynamics, Thermocline Adjustment, and Regulation of Tropical SST. *J. Climate*, 10, 521–534.
- Sengupta, D. and Ravichandran, Oscillations of Bay of Bengal sea surface temperature during the 1998 summer monsoon, *Geophys. Res. Lett.*, 28, (10), 2033–2036, 2001.

- Sengupta, D., B. N. Goswami and R. Senan, Coherent Intraseasonal Oscillations of Ocean and Atmosphere during the Asian Summer Monsoon, *Geophys. Res. Lett.*, *28*, (21), 4127–4130, 2001.
- Sengupta, D., P. K. Ray, and G. S. Bhat, Spring warming of the eastern Arabian Sea and Bay of Bengal from buoy data, *Geophys. Res. Lett.*, *29*, (15), 10.1029/2002GL015340, 2002.
- Sengupta, D., G. N. Bharath Raj, and S. S. C. Shenoi, Surface freshwater from Bay of Bengal runoff and Indonesian Throughflow in the tropical Indian Ocean, *Geophys. Res. Lett.*, *33*, L22609, 10.1029/2006GL027573, 2006.
- Shankar, D., P. N. Vinayachandran, A. S. Unnikrishnan and S. R. Shetye, The Monsoon Currents in the North Indian Ocean, *Progr. Oceanogr.*, *1*, 63–119, 2002.
- Shankar, D., V. V. Gopalakrishna, S. S. C. Shenoi, F. Durand, S. R. Shetye, C. K. Rajan, Z. Johnson, N. Araligidad, and G. S. Michael, Observational evidence for westward propagation of temperature inversions in the southeastern Arabian Sea, *Geophys. Res. Lett.*, *31*, L08305, 2004.
- Shenoi, S. S. C., D. Shankar, and S. R. Shetye, On the sea surface temperature high in the Lakshadweep Sea before the onset of the southwest monsoon. *Geophys. Res. Lett.*, *104*, 15703–15712, 1999.
- Shenoi, S. S. C., D. Shankar, and S. R. Shetye, Difference in the heat budgets of the near-surface Arabian Sea and Bay of Bengal: Implications for the summer monsoon, *Geophys. Res. Lett.*, *107*, No. C6, doi:10.1029/2000JC000679, 2002.
- Shenoi, S. S. C., D. Shankar, and S. R. Shetye, Remote forcing annihilates barrier layer in the southeastern Arabian Sea, *Geophys. Res. Lett.*, *31*, doi:10.1029/2003GL019270, 2004.

- Shinoda, T., Impact of the diurnal cycle of solar radiation on intraseasonal SST variability in the western Equatorial Pacific *J. Climate*, 18, 2628–2636, 2005.
- Shinoda, T., H. H. Hendon and J. Glick, Intraseasonal Variability of surface fluxes and sea surface temperature in the Tropical Western Pacific and Indian Oceans. *J. Climate*, 11, 1685–1702, 1998.
- Shinoda, T., and H.H. Hendon, 1998: Mixed Layer Modeling of Intraseasonal Variability in the Tropical Western Pacific and Indian Oceans. *J. Climate*, 11, 2668–2685, 1998.
- Siegel, D. A., et al., Solar radiation, phytoplankton pigments and the radiant heating of the equatorial Pacific warm pool, *J. Geophys. Res.*, 100, 4,885–4,892, 1995.
- Slingo, J. M., P. M. Inness and K. R. Sperber, Modeling, *in* Intraseasonal Variability in the Atmosphere - Ocean Climate System, W. K. M. Lau and D. Waliser (Eds.), pp 361–388, Springer, 2005
- Sun, D. Z and Z. Liu, Dynamic Ocean-Atmosphere Coupling: A Thermostat for the Tropics, *Science*, 272, 1148, 1996
- Turner J. S., Buoyancy effects in fluids, *Cambridge University Press*, pp. 367, 1973.
- Vinaychandran, P. N., D. Shankar, J. Kurian, F. Durand and S. S. C. Shenoi, Arabian Sea mini warm pool and monsoon vortex. *Curr. Sci.*, 93, 203–214, 2007.
- Wallace, J. M., Effect of deep convection on the regulation of tropical sea surface temperature *Nature*, 357, 230–231, 1992.
- Wang B., Theory, *in* Intraseasonal Variability in the Atmosphere - Ocean Climate System, W. K. M. Lau and D. Waliser (Eds.), pp 307–360, Springer, 2005
- Webster, P. J., V. O. Magana, T. N. Palmer, J. Shukla, R. A. Thomas, M. Yanai, and T. Yasunari, Monsoons: Processes, predictability, and the prospects for prediction, *J. Geophys. Res.*, 103(C7), 14,451–14,510, 1998.

- Webster P. J., A. M. Moore, J. P. Loschnigg and R. R. Leben, Coupled ocean-atmosphere dynamics in the Indian Ocean during 1997, *Nature*, 401, 356–360, 1999.
- Weller, R. A., A. S. Fischer, D. L. Rudnick, C. C. Eriksen, T. D. Dickey, J. Marra, C. Fox, and R. Leben (2002), Moored observations of upper-ocean response to the monsoons in the Arabian Sea during 1994-1995, *Deep Sea Res. II*, 49, 2195– 2230.
- Woods, J., Laminar flow in the ocean Ekman Layer, *Meteorology at the Millennium, Ed: R.P. Pearce, Acad. Press*, 220–232, 2002.
- Houghton, D. and Woods, J., The slippery seas of Acapulco, *New Scientist*, 134–136, 1969.
- Zhang, C., and M.J. McPhaden, Intraseasonal Surface Cooling in the Equatorial Western Pacific. *J. Climate*, 13, 2261–2276, 2000.
- Zeng, X., M. Zhao and R. E. Dickinson, Intercomparison of bulk aerodynamic algorithms for the computation of sea surface fluxes using TOGA COARE and TAO data, *J. Climate*, 11, 2628–2644, 1998.

	Q_{sw}^{net}	Q_{lw}^{net}	Q_{lat}	Q_{net}	Q_{pen}	Q_{eff}	Q_{adv}
Phase I	241	-46	-84	105	-79	26	5
Phase II	243	-56	-154	25	-68	-43	-85

Table 1. Mean heat fluxes (W/m^2) and mixed layer depth (m), and net temperature change ($^{\circ}\text{C}$) during the warming period 21-27 April (phase I) and cooling period 30 April-2 May (phase II).

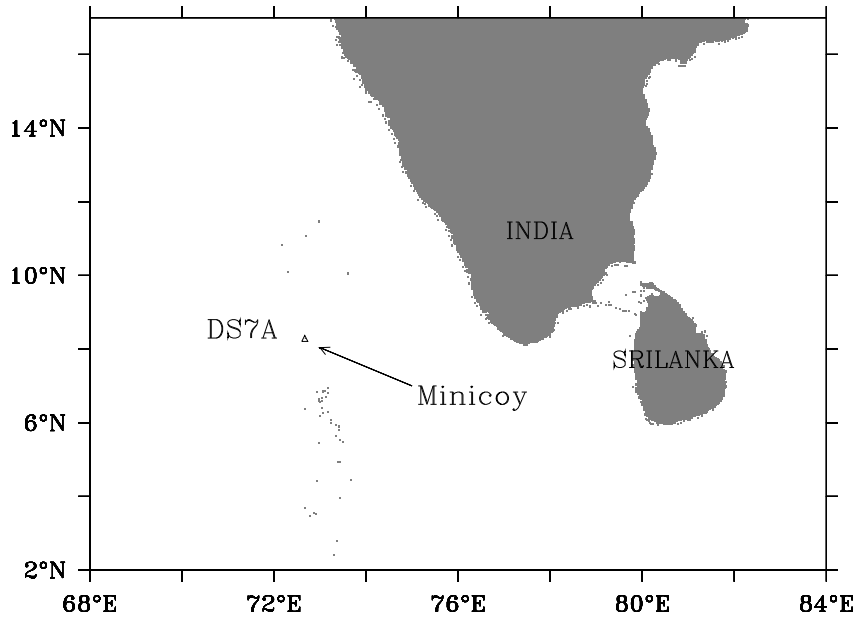


Figure 1. Region of the ARMEX process study. The triangle marks the location of mooring DS7A (8.3°N, 72.67°E). The tip of the arrow indicates the the island of Minicoy, ~40 kms from DS7A.

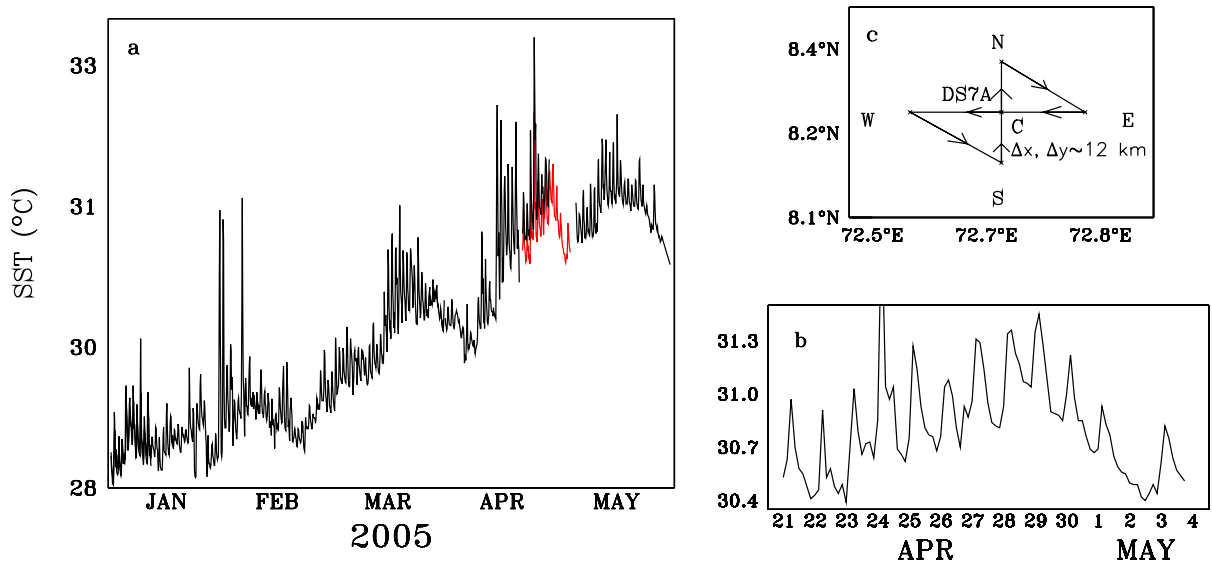


Figure 2. (a) January-May 2005 SST (~ 2 m temperature) from buoys DS7 (black) and DS7A (red). (b) DS7A SST during the ARMEX process study, 21 April to 4 May 2005. (c) Repeat ship track and CTD stations N, S, E, W and C; the distance between E and W, or N and S, is ~ 12 km; DS7 and DS7A are located near C.

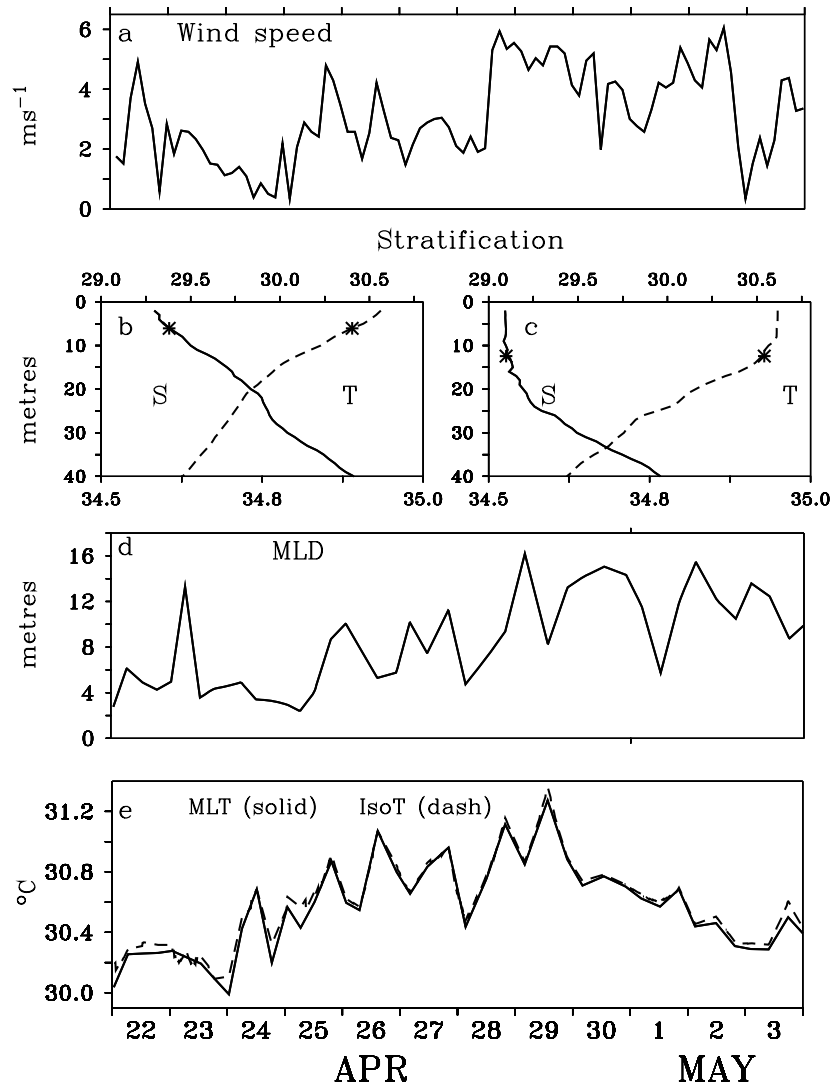


Figure 3. (a) Wind speed (m/s) from DS7A. (b) CTD salinity (solid; scale on lower x-axis) and temperature ($^{\circ}\text{C}$; dashed) profiles averaged over phase I. (c) As in (b), but for phase II; the star marks the mean mixed-layer depth (m) from CTD data. (d) Time variation of mixed-layer depth $D(t)$ (m). (e) Vertical mean temperature in the mixed layer ($\rho_{2m} + 0.05 \text{ kg/m}^3$) MLT (solid), and the isothermal layer ($SST - 0.25^{\circ}\text{C}$) IsoT (dashed).

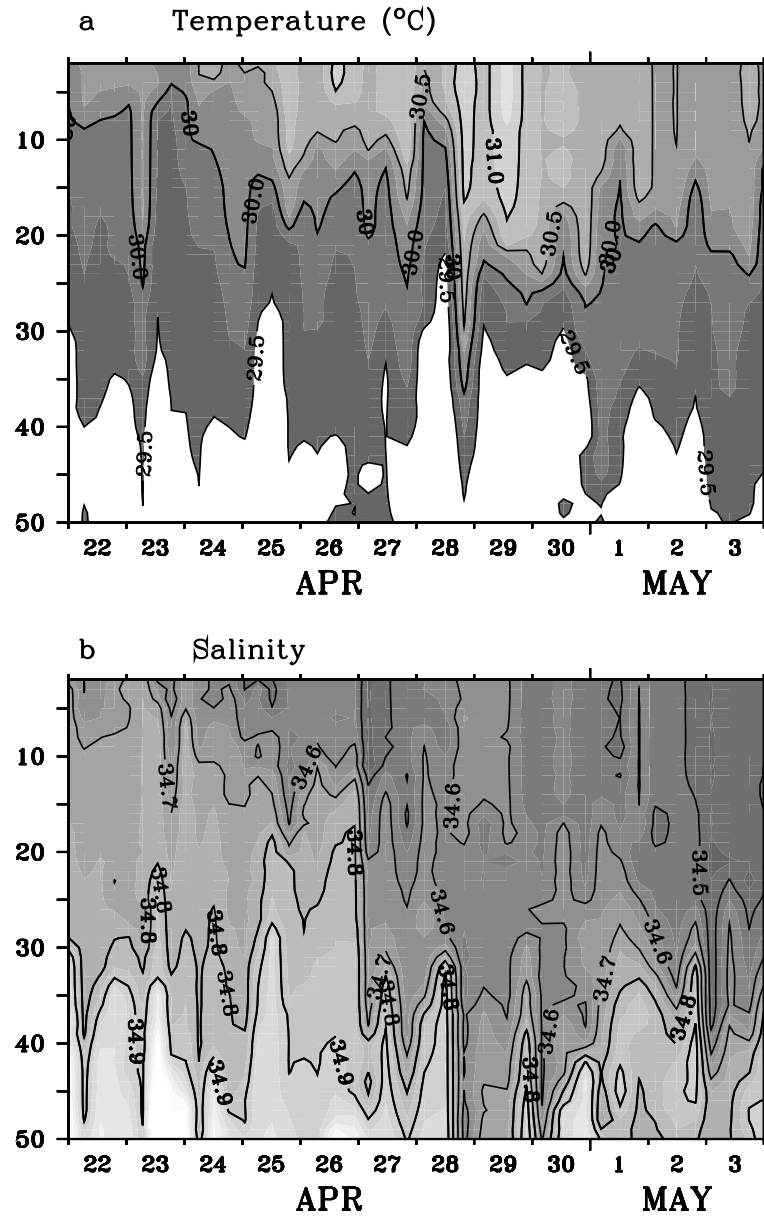


Figure 4. (a) Upper ocean temperature (°C) and (b) salinity (psu) as functions of depth and time, from CTD observations at station C.

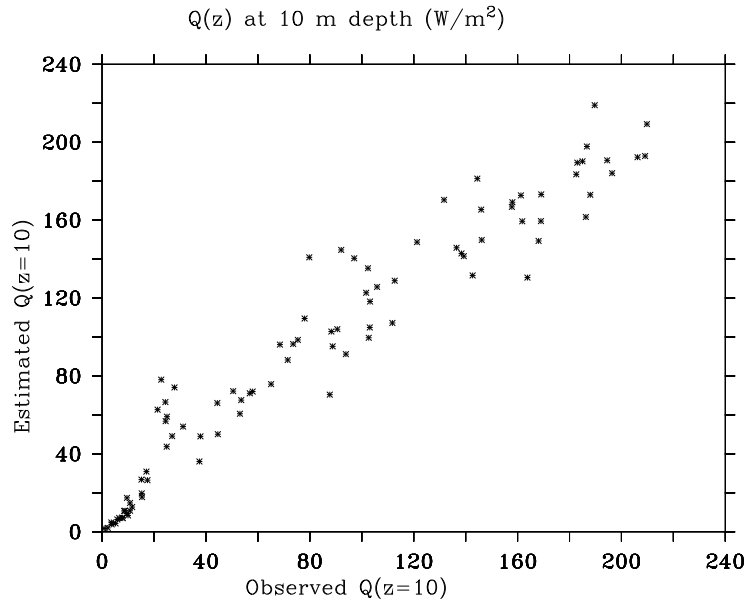


Figure 5. Scatter plot of directly measured and estimated penetrative shortwave flux, $Q(z)$ (W/m^2) at 10 m depth. The measurements of $Q(z)$ come from 101 casts of the subsurface radiometer at two time series stations occupied in ARMEX 2003 (17 May - 5 Jun 2003), while the estimates are based on co-located shipboard surface radiation measurements. The root-mean-square scatter is $17 W/m^2$

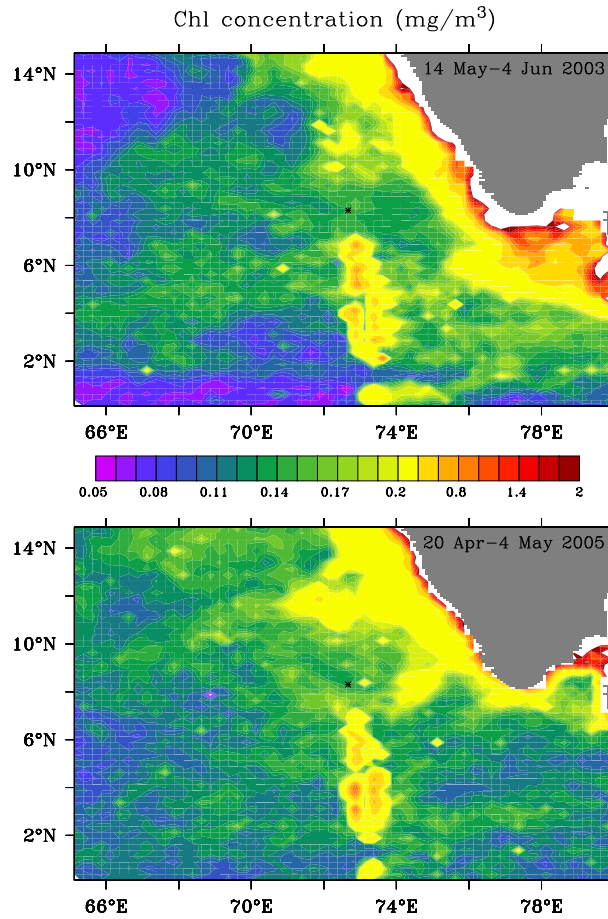


Figure 6. Weekly Chlorophyll concentration (mg/m^3) from SeaWiFS, averaged over 11 May-7 Jun 2003 and 17 April-7 May 2005, approximately coinciding with the ARMEX 2003 and 2005 campaigns (top right of each panel). The ARMEX location is marked by a black dot.

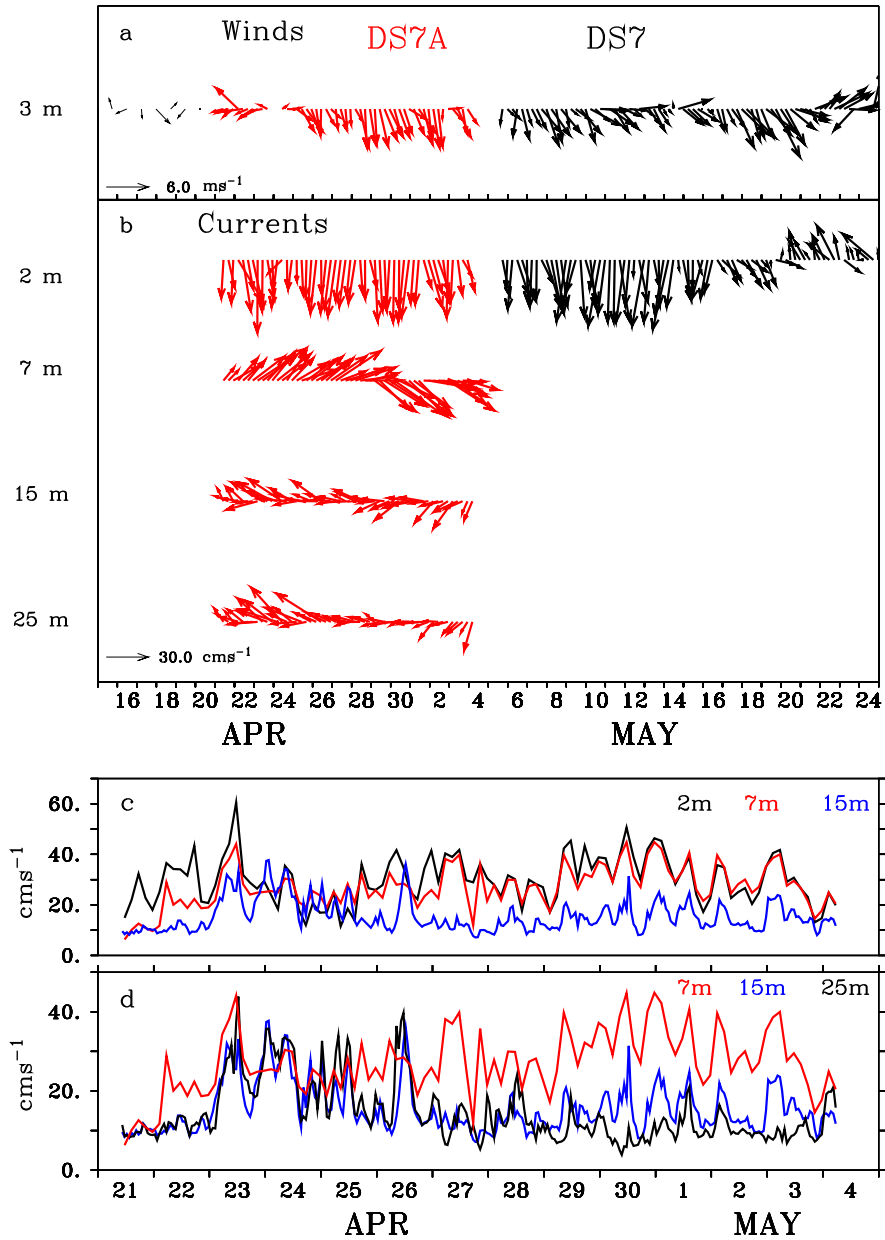


Figure 7. (a) Winds at ~ 3 m height from DS7 (black) and DS7A (red); the arrow at the bottom represents windspeed of 6 m/s. (b) Currents at ~ 2 m depth from DS7 (black), and currents from DS7A (red) at 2, 7, 15 and 25 m depth from 21 April to 4 May 2005; the arrow at the bottom represents 30 cm/s current speed. (c) Current speed (cm/s) at 2 m (black), 7 m (red), and 15 m (blue) from DS7A. (d) As in (c), but for 7 m (red), 15 m (blue) and 25 m (black).

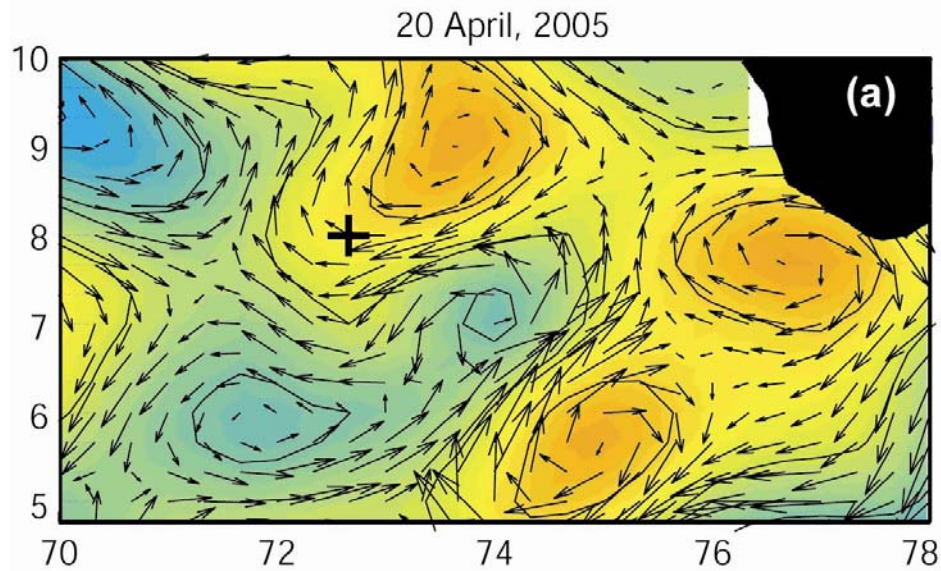


Figure 8. Ten day satellite Sea Surface Height Anomaly (SSHA, cm) for the period 15-25 April 2005 in the southeastern Arabian Sea, with geostrophic current vectors superimposed. The difference between the bright orange and blue shades is about 18 cm (adapted from *Murty et al* [2006]).

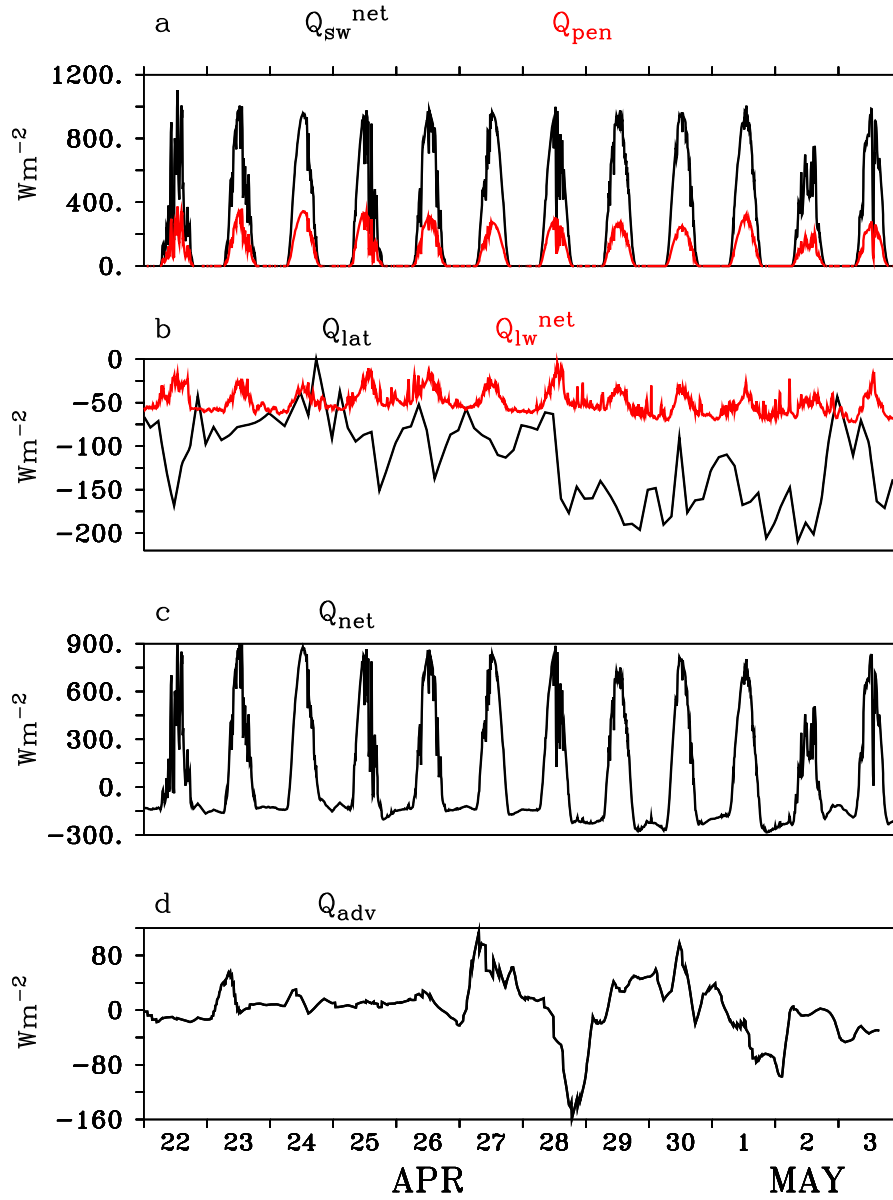


Figure 9. Heat fluxes (W/m^2). (a) Net surface shortwave radiation Q_{SW}^{net} (black) and shortwave flux penetrating below the mixed layer Q_{pen} (red). (b) Latent heat flux Q_{lat} (black) and net outgoing longwave radiation Q_{lw}^{net} (red). (c) Net heat flux Q_{net} , and (d) Lateral advection Q_{adv} .

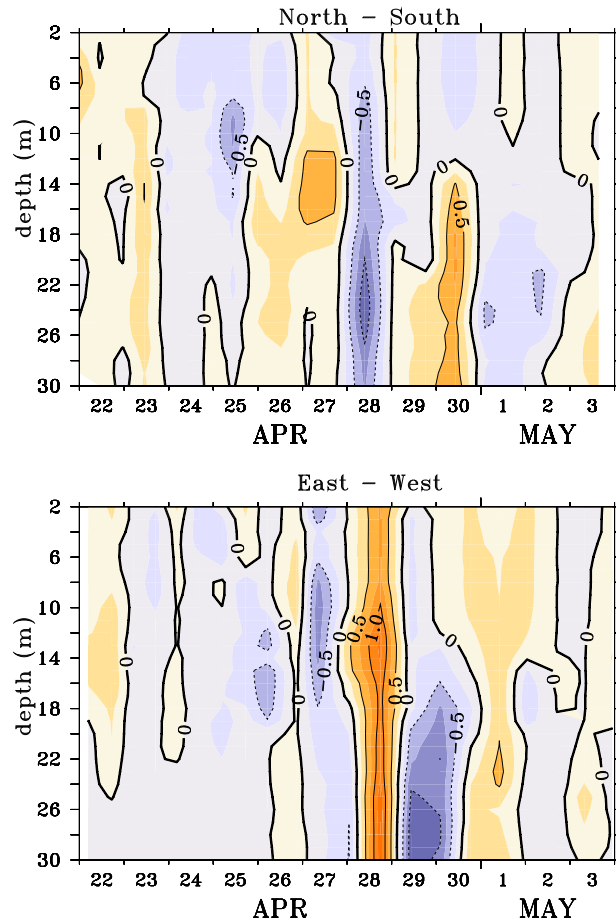


Figure 10. Temperature difference ($^{\circ}\text{C}$) in the upper 30 m in (a) meridional (North-South) and (b) zonal (East-West) directions.

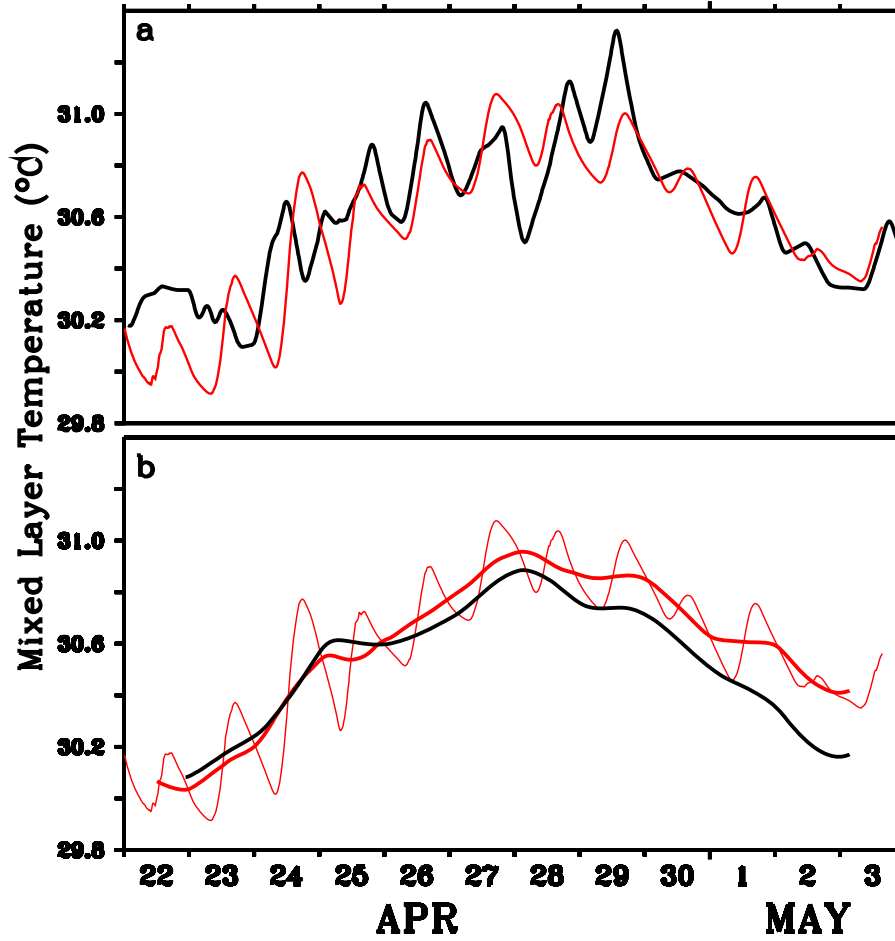


Figure 11. (a) Mixed-layer temperature (MLT; °C) from CTD observations (black), and from estimates (red) based on Q_{net} , Q_{pen} and Q_{adv} . (b) Estimated MLT (as in (a); thin red), smoothed (24-hour running mean) estimated MLT (bold red), and MLT calculated from smoothed $D(t)$ and fluxes (black).

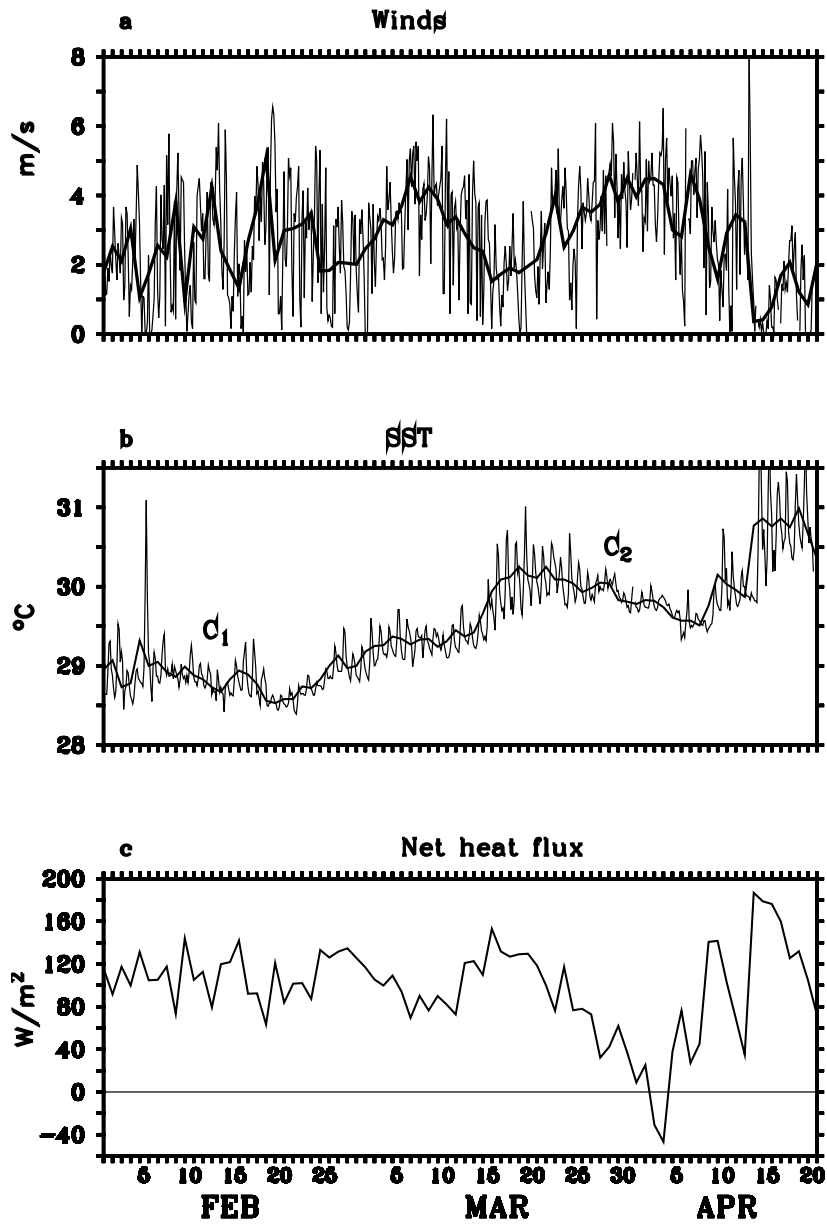


Figure 12. Two subseasonal cooling events, C_1 (1-20 Feb 2005) and C_2 (20 Mar-8 Apr) in DS7 SST. Daily mean (thick) and 3 hourly (thin) measurements of (a) wind speed (m/s) and (b) SST ($^{\circ}\text{C}$). (c) Daily net heat flux into the ocean (W/m^2).

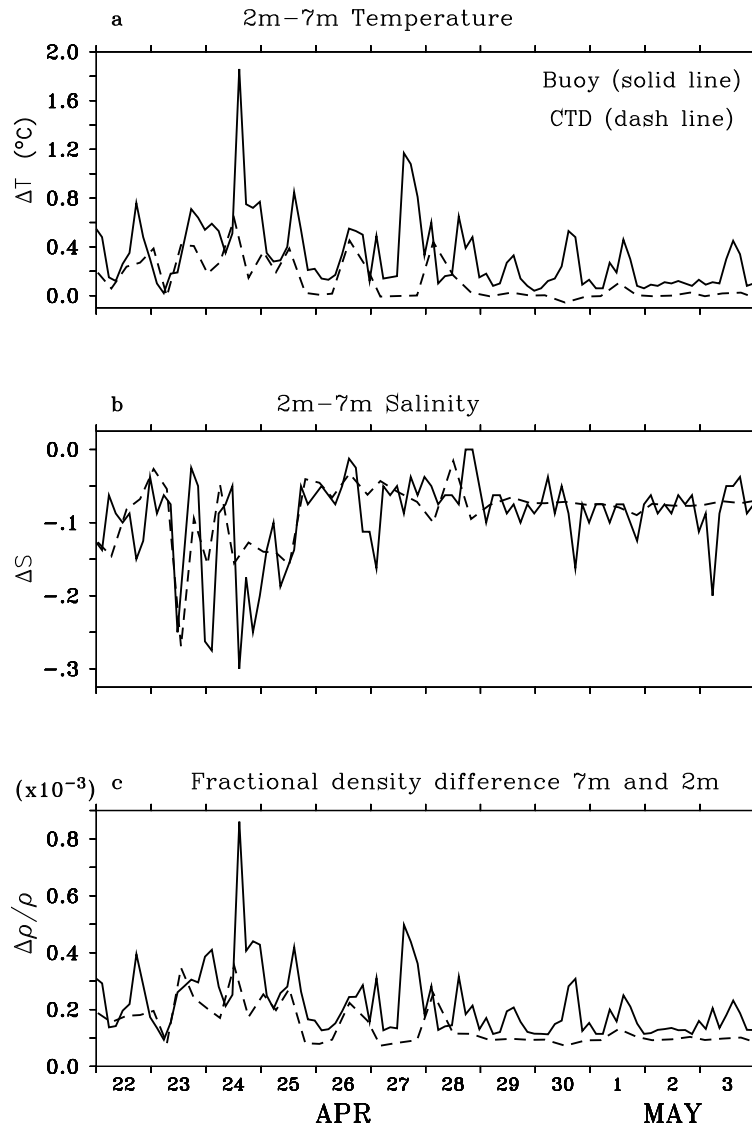


Figure 13. (a) Difference in 2 m and 7 m temperature ($^{\circ}\text{C}$) from buoy DS7A (solid) and CTD (dashed) observations. (b) As in (a), but for salinity. (c) Fractional density difference $\Delta\rho/\rho$ (10^{-3} kg/m^3) between 7 m and 2 m depth, from buoy (solid) and CTD (dashed). The persistent minimum density difference of $\sim 0.1 \text{ kg/m}^{-3}$ is mainly due to salinity stratification.

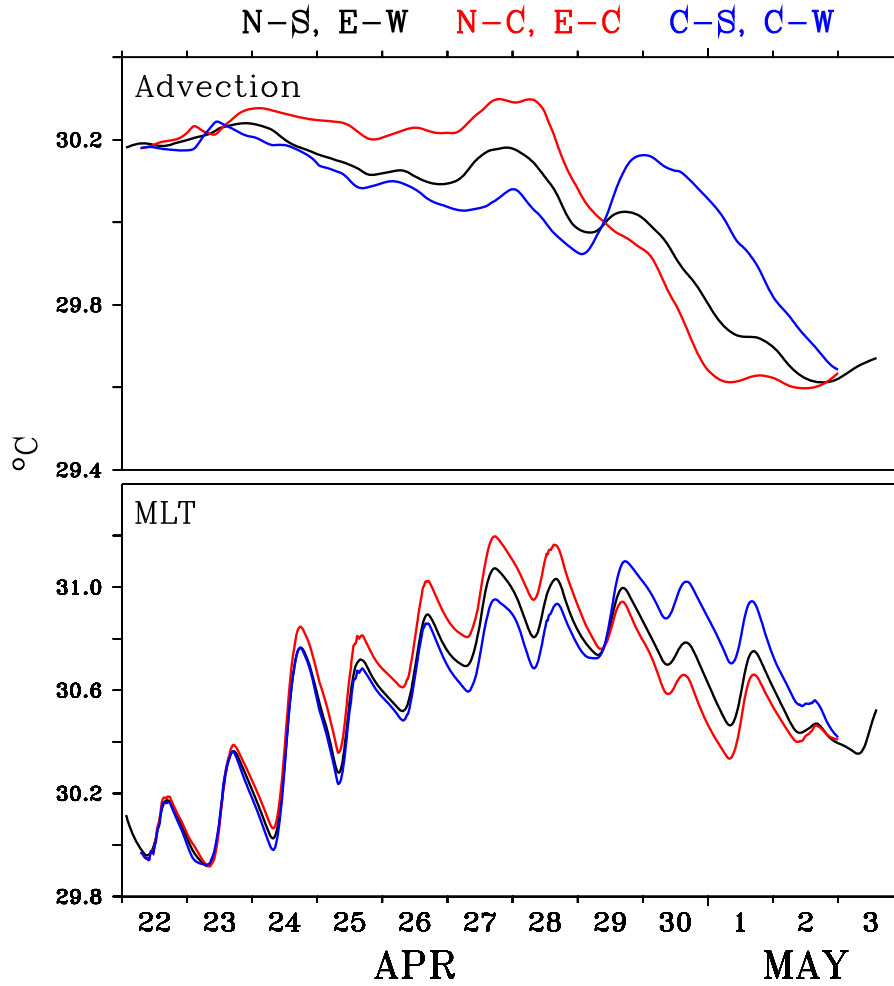


Figure 14. Sensitivity of lateral advection to non-uniform temperature gradients within the ARMEX array. (a) Advection ($^{\circ}\text{C}$) with meridional T gradient ($\frac{\partial T}{\partial y}$) and zonal T gradient ($\frac{\partial T}{\partial x}$) estimated from North-South and East-West (N-S, E-W; black) CTD stations; from North-Centre and East-Centre (N-C, E-C; red), and Centre-South and Centre-West (C-S, C-W; blue). (b) Mixed layer temperature (MLT) computed using the three estimates of temperature gradient in (a): N-S, E-W (black), N-C, E-C (red) and C-S, C-W (blue).

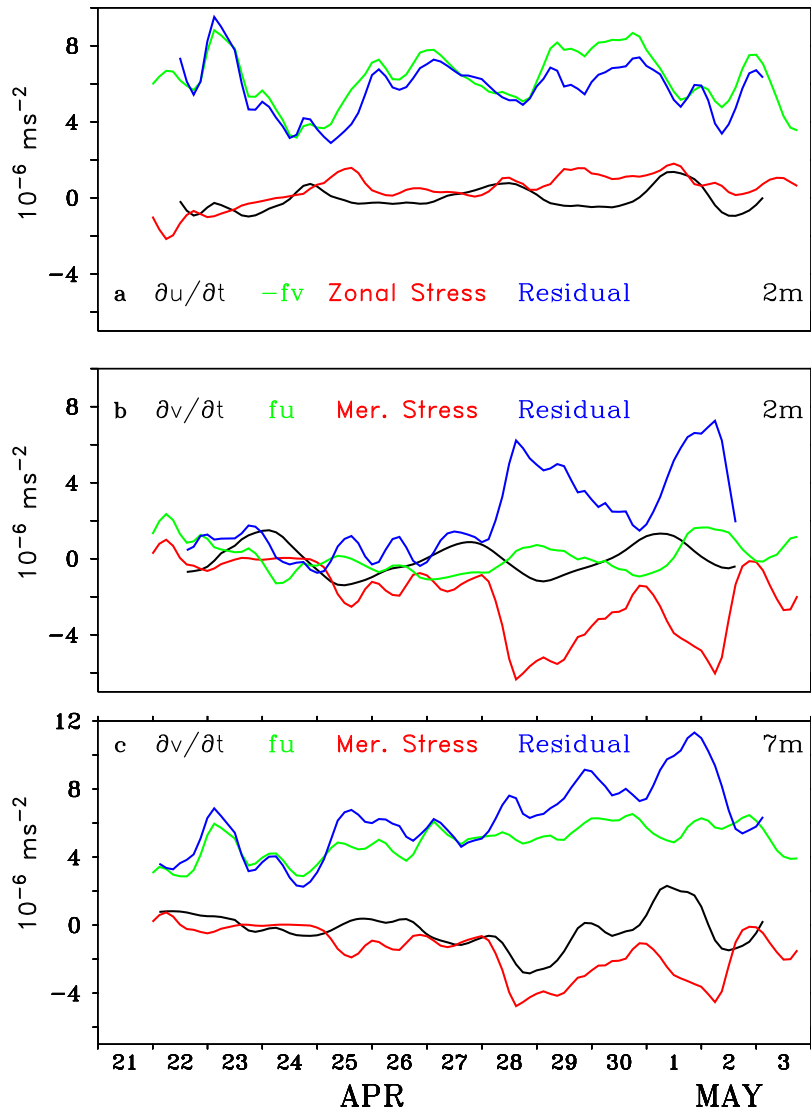


Figure A1. (a) Local (black) and coriolis (green) zonal acceleration in the upper 6 m (based on 2 m currents); acceleration due to estimated stress (red) in the upper 6 m; and the residual (blue) of these three terms from the momentum balance (Eq A1). (b) As in (a) but for meridional acceleration. (c) As in (b), except for the 6-14 m layer (based on 7 m currents). Acceleration is in 10^{-6} m/s^2 .